Title	Collapse of surface nanobubbles
Author(s)	Chan, Chon U.; Chen, Longquan; Arora, Manish; Ohl, Claus-Dieter
Citation	Chan, C. U., Chen, L., Arora, M., & Ohl, C. D. (2015). Collapse of surface nanobubbles. Physical review letters, 114(11).
Date	2015
URL	http://hdl.handle.net/10220/25394
Rights	© 2015 American Physical Society. This paper was published in Physical Review Letters and is made available as an electronic reprint (preprint) with permission of American Physical Society. The paper can be found at the following official DOI: [http://dx.doi.org/10.1103/PhysRevLett.114.114505]. One print or electronic copy may be made for personal use only. Systematic or multiple reproduction, distribution to multiple locations via electronic or other means, duplication of any material in this paper for a fee or for commercial purposes, or modification of the content of the paper is prohibited and is subject to penalties under law.

Collapse of Surface Nanobubbles

Chon U. Chan, Longquan Chen, Manish Arora, and Claus-Dieter Ohl*
School of Physical and Mathematical Science, Nanyang Technological University, 21 Nanyang Link, 637371 Singapore
(Received 14 November 2014; published 19 March 2015)

Surface attached nanobubbles populate surfaces submerged in water. These nanobubbles have a much larger contact angle and longer lifetime than predicted by classical theory. Moreover, it is difficult to distinguish them from hydrophobic droplets, e.g., polymeric contamination, using standard atomic force microscopy. Here, we report fast dynamics of a three phase contact line moving over surface nanobubbles, polymeric droplets, and hydrophobic particles. The dynamics is distinct: across polymeric droplets the contact line quickly jumps and hydrophobic particles pin the contact line, while surface nanobubbles rapidly shrink once merging with the contact line, suggesting a method to differentiate nanoscopic gaseous, liquid, and solid structures. Although the collapse process of surface nanobubbles occurs within a few milliseconds, we show that it is dominated by microscopic dynamics rather than bulk hydrodynamics.

DOI: 10.1103/PhysRevLett.114.114505 PACS numbers: 47.55.D−, 47.55.np, 47.61.−k

The decoration of wetted surfaces with nanoscopic gaseous bodies would have important consequences for drag reduction in micro- and nanofluidics [1–3]. The existence of these surface attached nanobubbles was first proposed by Parker *et al.* to explain the long-ranged (∼100 nm) attraction force between two hydrophobic surfaces immersed in water [4]. Since then, evidence of surface nanobubbles was documented intensively using various techniques including atomic force microscopy (AFM) [5,6], x-ray reflectivity measurements [7,8], infrared spectroscopy [9,10], and optical microscopy [11–13]. The general finding is that surface nanobubbles have large nanoscopic contact angles and they can survive for hours and even up to days [14,15].

The long lifetime is a puzzling property of surface nanobubbles. Theoretically, small bubbles with radii of curvature of less than 1 μm should dissolve in water within microseconds [16], while in experiments surface nanobubbles dissolve much slower than expected [14,15]. Currently, their stability is explained theoretically either with a dynamic equilibrium model accounting for recirculation of gas [17,18] or the far-field length scale for gas diffusion [19]. These models assume cooperative effects of the nanobubble clusters and/or the pinning of their contact lines.

Nanoscopic bubbles are difficult to identify with current methods: imaging techniques such as AFM and optical microscopy cannot unambiguously identify their gaseous content [9,20] while conflicting results were obtained with other techniques [7–10,21–26]. Some authors postulated that the long-living nanoscopic objects are polymeric contaminants [20,21,22, 23,24]. Indeed, surface nanobubblelike objects were observed in recent experiments on highly ordered pyrolytic graphite using AFM, which ultimately turned out to be polydimethylsiloxane (PDMS) contamination from coated sterile needles [27,28]. Therefore, it is paramount to be able to distinguish surface nanobubbles from contaminations.

In this Letter, we comparatively study the interaction of receding contact lines (CLs) with surface nanobubbles, polymeric droplets, and solid particles. Surface nanobubbles spontaneously collapse once the receding CL touches them, while a fast receding process and a pinning-depinning process are observed on polymeric droplets and on solid particles, respectively. These distinct dynamics offer a potential technique to identify surface nanobubbles.

The experimental procedure to generate surface nanobubbles is the well known water-ethanol-water exchange procedure [15] conducted in microchannels. The subsequent replacement of ethanol by water leads to nanobubble nucleation on the glass surface as the solubility of gas or air in water is much smaller than in ethanol [15]. On the clean glass surface, we measured an equilibrium water contact angle $\theta_{eq} = 21.7° \pm 1.7°$ and an advancing water contact angle $\theta_{ad} = 39.4° \pm 1.0°$. However, we did not obtain a receding contact angle θ_{re} since the contact line does not recede and even the water was almost completely withdrawn. Both the deionized water and the ethanol contain 5 μM rhodamine 6G fluorescent dye, which is surface active and allows for the observation of surface nanobubbles with a total-internal-reflection-fluorescence (TIRF) microscopy [11], as shown in Fig. 1. The polymeric contamination was created by electrospraying PDMS droplets onto glass surfaces [29]. The resulting size of the deposited PDMS droplets varies largely, yet some of the small droplets have radii down to 2.0 μm. To simulate solid contamination, monodisperse polystyrene particles labeled with red fluorescent dye were dip coated on glass surfaces. The radius of these particles is 0.5 μm. We controlled the receding speed of the contact line over the surface nanobubbles by slowly pumping air into the microchannel (Fig. 1). For PDMS droplets and polystyrene particles,

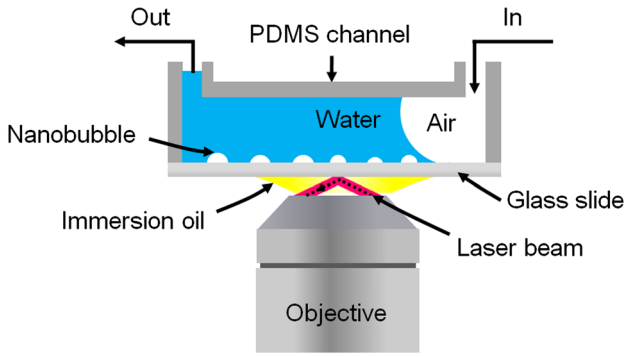

FIG. 1 (color online). Schematic of the TIRF microscopy used to observe receding CL over surface nanobubbles and PDMS droplets.

the receding speed was monitored by evaporating 4 μL water droplets deposited on them. Details about the experimental setups and procedures are stated in the Supplemental Material [30].

Gaseous bodies.—TIRF microscopy reveals disk-shaped objects with radii of 0.2–1.0 μm on the glass surface following the solvent exchange process. Below we identify these objects as surface nanobubbles. A typical configuration is depicted in the left image of Fig. 2(a). Large disk objects have a higher intensity near their edges while being dimmer at their center, indicating that they are more distant from the substrate at their center [11]. As the evanescent light intensity decays exponentially from the water-glass interface [31], we estimated with the given experimental parameters a height of several tens of nanometers for these objects.

The right frames of Fig. 2(a) display the dynamics process of a receding CL traveling from right to left across one of the bright objects: The speed of the CL is $\sim$0.52 μm/s before it touches the bright disk with a radius of 0.45 μm, and these four frames are selected from a movie recorded at 46 frames/s. At the moment the CL reaches the object, it shrinks abruptly and its brightness changes, which is already visible at $t = 22$ ms. Because of motion blurring we cannot infer the height of the bubble from the brightness of the pixels. At $t = 44$ ms, the disk shrinks to a smaller one with a radius of $\sim$0.15 μm [marked with a dotted circle in Fig. 2(a)] and the small disk disconnects from the CL. Only when the CL touches the object again (after about 1 s) does it shrink and vanish (within one frame; see movie M1 in the Supplemental Material [30]). Similar multistep collapse processes were observed for larger objects, while single collapse processes were only observed for small objects; see movie M1 [30].

The shrinkage and disappearance of the object in combination with the particular dynamics of the CL indicate that we are observing the shrinking of a surface attached bubble with an initial height of several tens of nanometers. Next we demonstrate that other objects such as polymeric droplets or solid particles show prominently different CL dynamics.

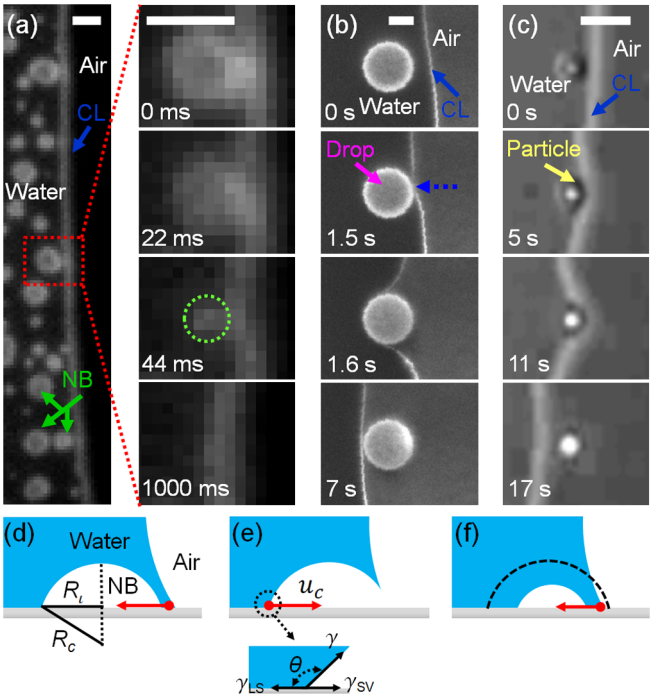

FIG. 2 (color online). Snapshots of a CL receding over (a) surface nanobubbles (NB), (b) a PDMS droplet, and (c) a colloidal particle. The CL receding speeds in (a)–(c) are 0.52, 0.60, and 0.40 μm/s, respectively. The lengths of the scale bars are in (a) 1 μm and in (b) and (c) 2 μm. (d)–(f) Sketch of the collapse dynamics of a surface nanobubble seen from the side.

Polymeric droplet contaminations can easily be obtained from nonclean working methods. They can result from hydrophobic silanized surfaces after contact with water [20] or be obtained from flow lines as recently reported [27,28]. Also, *solid* contaminations originating from the solvent were reported in nanobubble research [21,32]. These contaminations have some properties such as nanoscopic size, shape, long lifetime (stability), and deformability [20,21,27,32] very much in common with nanobubbles. In the following, we show first the dynamic process of a receding CL moving over a PDMS droplet and then over a solid particle.

Hydrophobic droplets.—The first frame of Fig. 2(b) depicts a 2.0 μm radius PDMS droplet submerged in water with the contact line at some distance to its right. The fluorescent dye from the water has diffused into the PDMS droplet which under TIRF illumination results in a similar appearance to the previously studied surface nanobubbles. In Fig. 2(b), from top to bottom, the CL moves with an initial speed of approximately 0.60 μm/s toward the left (see movie M2 in the Supplemental Material [30]). The hydrophobic droplet on a hydrophilic glass surface leads to a local decrease of the interfacial energy and changes the local surface wettability [33,34]. When the CL is far away from the droplet, its receding speed is almost uniform everywhere. However, at a distance of $\sim$1.0 μm from the

droplet's edge, the CL region closest to the droplet recedes faster than other regions [marked with an arrow in Fig. 2(b)]. This suggests that a hydrophobic precursor film exists around the PDMS droplet [33,34]. Once the CL near the droplet meets the droplet's edge, the CL quickly traverses the droplet, here within 0.1 s [see $t = 1.5$ to 1.6 s in Fig. 2(b)]. Then, the CL passes the droplet and remains fixed until the outer slowly moving sections catch up; see $t = 7$ s in Fig. 2(b).

Solid particles.—The receding process of a CL toward a 0.5 m radius solid particle at a speed of 0.40 μm/s with selected frames is shown in Fig. 2(c) and in movie M3 in the Supplemental Material [30]. Again a uniformly receding CL is observed far from the particle. However, once it reaches the particle, the CL near the particle is anchored due to the adhesive pinning force; see $t = 5$ s in Fig. 2(c). As a result, the retreating speed is slowed down and the CL is deformed. With further receding of the CL, the region closest to the particle becomes highly bent [$t = 11$ s in Fig. 2(c)], which in turn results in an increase of the capillary force toward the receding direction of the CL. Once this capillary force is larger than the pinning force, the CL depins from the particle. Eventually, a uniformly receding CL is recovered at $t = 17$ s in Fig. 2(c).

As described above, a fast jump and a pinning-depinning behavior of the CL are observed when the CL recedes over a polymeric droplet and a solid particle, respectively. In both cases, the objects remain fixed when the CL passes by, as shown in Figs. 2(b) and 2(c) (although we are aware of the possibility of detachment and transport of particles by the moving CLs). In contrast, the nanobubbles in Fig. 2(a) exhibit typical properties of gaseous bodies being exposed to ambient atmosphere: shrinking and complete removal [33]. These distinct qualities can be used to identify surface nanobubbles.

To study the process of nanobubble shrinkage in greater detail, we utilize a high-speed camera. The rather weak fluorescent signal limits the maximum framing rate to 2000 fps. Unfortunately, due to the larger pixel size of that camera at the same magnification, each nanobubble is now captured with only a few pixels (see movie M4 in the Supplemental Material [30]). Although we do not have the spatial resolution to trace the instantaneous lateral radius, we can study the temporal dynamics of the collapse by analyzing the averaged pixel intensity in the region of surface nanobubbles (details are available in the Supplemental Material [30]). Figure 3 shows the average pixel intensity $I(t)$ as a function of time for selected nanobubbles with an initial lateral radius R_l of 0.38–0.56 μm. The intensity I is about constant when the CL is away from the surface nanobubble. However, once the CL meets the bubble, the surface nanobubble shrinks and thus its averaged intensity decreases. Zooming temporally into the intensity curves during the collapse (inset of Fig. 3) reveals that the shrinkage is fast in the beginning and slows down as the intensity I approaches a new constant value. For large bubbles we observe multistep collapses while small bubbles only shrink once.

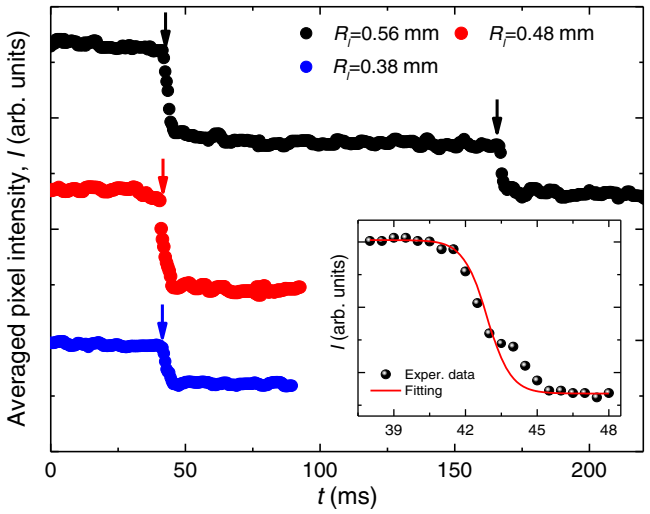

FIG. 3 (color online). Averaged pixel intensity I of nanobubbles as a function of time t. The inset shows the change of I during the rapid shrinkage of a nanobubble with $R_l = 0.38$ μm. The arrows mark the time the collapse process starts.

The obvious question to ask is the following: What forces govern the collapse of the surface nanobubble? Our hypothesis is sketched in Figs. 2(d)–2(f). Because of Laplace pressure [33], the gas pressure inside the nanobubble is higher than the pressure in the gas phase behind the contact line. This pressure difference can be quantified by assuming the shape of the nanobubble being a spherical cap with a radius R_c with $\Delta P = 2\gamma/R_c$, where γ is the surface tension. When the CL approaches the surface nanobubble, the liquid film separating the bubble and ambient atmosphere thins and eventually ruptures [Fig. 2(d)]. As a result, the gas can escape and the pressure inside and outside the bubble equilibrates [Fig. 2(e)]. Since the nanoscopic contact angle of the surface nanobubble θ (water side) is much larger than the equilibrium contact angle [15,35] θ_{eq}, the interfacial tensions γ, γ_{LS}, and γ_{SV} at the liquid-solid-vapor CL of the nanobubble are not balanced [Fig. 2(e)]. In this nonequilibrium state, a net capillary force (per unit length) $\gamma(\cos\theta_{\mathrm{eq}} - \cos\theta)$ acts on the CL of the nanobubble, which leads to the shrinkage of the nanobubble and the movement of the nanobubble CL. With ongoing shrinking, the contact angle decreases; the capillary force decreases, and thus the shrinking speed should decrease. This may indeed be observed in the experiment as a slow decay of signal in Fig. 3, yet we cannot rule out other processes such as gas diffusion or diffusion of the fluorescent dye which may lead to a similar signal. If the nanobubble size is small, the air inside the bubble can be completely squeezed out and the bubble vanishes. However, if the bubble size is sufficiently

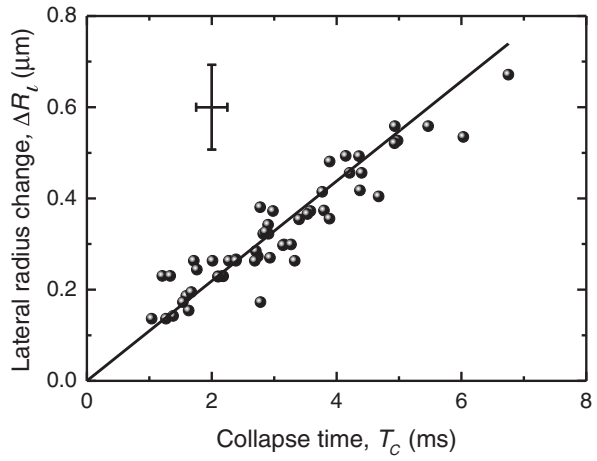

FIG. 4. Collapse time T_c as a function of the lateral radius change ΔR_l. The solid line is a linear fit, *i.e.*, $T_c = (1/u_c)\Delta R_l$.

large, the hole connecting the bubble and atmosphere can be closed again as the bubble region close to the CL shrinks backwards, leaving a daughter bubble [Fig. 2(f)]. This phenomenon has some similarity with the bubble entrapment during drop impact on solid surfaces [36].

The collapse dynamics indicates that the state of surface attached nanobubbles, i.e., high pressure with large microscopic contact angle, is energetically in a metastable state. Under perturbations, like here exposing the content to ambient atmosphere, it will develop into a new configuration. It is likely that the pinning force, which supports the large contact angle, is reduced. We want to point out that the CL interaction with surface attached nanobubbles under room temperature is different from the higher temperature phenomenon recently reported by Zhang *et al.*[13]. In their case, the vapor pressure which is comparable to the atmospheric pressure may have a stabilizing contribution, i.e., prevents the nanobubble collapse [13].

We now estimate a time scale for the nanobubble collapse T_c in the present experiments from the decrease of the spatially averaged intensity signal by fitting the experimental data with a smooth step function: $I(t) = (I_f - I_i)/2 \tanh[2(t - t_0)/T_c] + (I_i + I_f)/2$, where the fitting parameters I_f and I_i are the final and initial intensities, respectively, and t_0 is the time of transition. As mentioned previously, most bubbles show a multistep collapse; thus, many of them shrink to a smaller radius. Therefore, we plot the time T_c from above fitting as a function of the lateral radius change ΔR_l (for details, see the Supplemental Material [30]) in Fig. 4. The collapse time T_c is a few milliseconds and increases linearly with the change of the lateral bubble size: $T_c = (1/u_c)\Delta R_l$, where u_c is equivalent to a speed of this collapse process. A linear regression of the data results in $u_c \approx 110$ μm/s. This collapse speed should be related to the speed of the moving nanobubble contact line. In hydrodynamics, the contact line dynamics is described by the type of forces resisting capillary force: if the inertial force is dominant, the contact line speed scales as $u_i \sim \sqrt{(\gamma/\rho L)}$ [33]; if the viscous force is dominant, the contact line speed scales as $u_v \sim (\gamma/\mu)$ [33,34], where ρ is the density of the liquid, L is the characteristic length, and μ is the bulk liquid viscosity. However, we find that both u_i and u_v are 5–6 orders of magnitude larger than the collapse speed obtained from Fig. 4. Therefore, bulk hydrodynamic processes cannot explain the collapse dynamics of the surface nanobubbles.

This inspired us to compare the speed scale observed with a microscopic model: the molecular kinetic theory [37,38]. Here, the contact line motion is described by the displacement of liquid molecules in the vicinity of a microscopic contact line [37,38]. While the contact line moves on a solid surface, the unbalanced capillary force $\gamma(\cos\theta_{\mathrm{eq}} - \cos\theta)$ drives the liquid molecules to hop over the energy barrier of wetting which is originated from the viscous friction among liquid molecules, and the adhesion between the solid and the liquid. The contact line speed is influenced by the heterogeneity of the solid surface (physical or chemical defects) [39], phase change (condensation or evaporation) near the contact line [40–42], and molecular slippage on the liquid-solid interface [43,44], and takes the form of $u_m = k(\gamma/\mu)(\cos\theta_{\mathrm{eq}} - \cos\theta)$ [37,38,45]. Where k is a nondimensional parameter determined by the factors, which influence the contact line motion as mentioned above, k has a value of the order of 10^{-6} for water on smooth surfaces [41,42]. Unfortunately, we do not know θ and cannot give a dynamic model of the motion, yet we can estimate it as $(\cos\theta_{\mathrm{eq}} - \cos\theta) \sim O(1)$, and thus, we obtain $u_m \sim 73\,\mu$m/s, which agrees surprisingly well with the measured collapse speed of 110 μm/s.

In summary, we have reported different dynamics of receding contact lines over surface nanobubbles, polymeric droplets, and solid particles. First, we found that surface nanobubbles show gaseous properties when they are exposed to atmosphere: they shrink and vanish. In contrast, fast receding and pinning-depinning processes were observed for polymeric droplets and solid particles, respectively. These findings may offer robust criteria to distinguish surface nanobubbles from liquid or solid contaminations in nanobubble research. Second, we found that the collapse of surface nanobubbles is much slower than bulk hydrodynamic scaling predicts and is in agreement with the molecular kinetic theory for contact line dynamics.

This work was stimulated by discussions with Detlef Lohse and Xuehua Zhang. C. U. C. and L. Q. C. contributed equally to the Letter. We gratefully acknowledge funding through Singapore National Research Foundation's Competitive research program (Program No. NRF-CRP9-2011-04).

*To whom all correspondence should be addressed.
cdohl@ntu.edu.sg

[1] C. Cottin-Bizonne, J.-L. Barrat, L. Bocquet, and E. Charlaix, Nat. Mater. **2**, 237 (2003).
[2] S. Granick, Y. X. Zhu, and H. Lee, Nat. Mater. **2**, 221 (2003).
[3] E. E. Meyer, K. J. Rosenberg, and J. Israelachvili, Proc. Natl. Acad. Sci. U.S.A. **103**, 15739 (2006).
[4] J. L. Parker, P. M. Claesson, and P. Attard, J. Phys. Chem. **98**, 8468 (1994).
[5] A. Carambassis, L. C. Jonker, P. Attard, and M. W. Rutland, Phys. Rev. Lett. **80**, 5357 (1998).
[6] J. W. G. Tyrrell and P. Attard, Phys. Rev. Lett. **87**, 176104 (2001).
[7] T. R. Jensen, M. Ostergaard Jensen N. Reitzel K. Balashev G. H. Peters K. Kjaer,and T. Bjornholm, Phys. Rev. Lett. **90**, 086101 (2003).
[8] M. Mezger, H. Reichert, S. Schoder, J. Okasinski, H. Schroder, H. Dosch, D. Palms, J. Ralston, and V. Honkimaki, Proc. Natl. Acad. Sci. U.S.A. **103**, 18401 (2006).
[9] X. H. Zhang, A. Khan, and W. A. Ducker, Phys. Rev. Lett. **98**, 136101 (2007).
[10] X. H. Zhang, A. Quinn, and W. A. Ducker, Langmuir **24**, 4756 (2008).
[11] C. U. Chan and C. D. Ohl, Phys. Rev. Lett. **109**, 174501 (2012).
[12] S. Karpitschka, E. Dietrich, J. R. T. Seddon, H. J. W. Zandvliet, D. Lohse, and H. Riegler, Phys. Rev. Lett. **109**, 066102 (2012).
[13] X. H. Zhang, H. Lhuissier, C. Sun, and D. Lohse, Phys. Rev. Lett. **112**, 144503 (2014).
[14] V. S. J. Craig, Soft Matter **7**, 40 (2011).
[15] J. R. T. Seddon and D. Lohse, J. Phys. Condens. Matter **23**, 133001 (2011).
[16] S. Ljunggren and J. C. Eriksson, Colloids Surf. A **129**, 151 (1997).
[17] M. P. Brenner and D. Lohse, Phys. Rev. Lett. **101**, 214505 (2008).
[18] N. D. Petsev, M. S. Shell, and L. G. Leal, Phys. Rev. E **88**, 010402(R) (2013).
[19] J. H. Weijs and D. Lohse, Phys. Rev. Lett. **110**, 054501 (2013).
[20] D. R. Evans, V. S. J. Craig, and T. J. Senden, Physica (Amsterdam) **339A**, 101 (2004).
[21] A. Habich, W. Ducker, D. E. Dunstan, and X. H. Zhang, J. Phys. Chem. B **114**, 6962 (2010).
[22] M. Mao, J. H. Zhang, R. H. Yoon, and W. A. Ducker, Langmuir **20**, 1843 (2004).
[23] A. Poynor, L. Hong, I. K. Robinson, S. Granick, Z. Zhang, and P. A. Fenter, Phys. Rev. Lett. **97**, 266101 (2006).
[24] Y. S. Seo and S. Satija, Langmuir **22**, 7113 (2006).
[25] R. Steitz, T. Gutberlet, T. Hauss, B. Klosgen, R. Krastev, S. Schemmel, A. C. Simonsen, and G. H. Findenegg, Langmuir **19**, 2409 (2003).
[26] Y. Takata, J. H. J. Cho, B. M. Law, and M. Aratono, Langmuir **22**, 1715 (2006).
[27] R. P. Berkelaar, E. Dietrich, G. Kip, H. Kooij, H. Zandvliet, and D. Lohse, Soft Matter **10**, 4947 (2014).
[28] H. J. An, G. M. Liu, and V. S. J. Craig, Adv. Colloid Interface Sci. (in press).
[29] S. J. Gaskell, J. Mass Spectrom. **32**, 677 (1997).
[30] See the Supplemental Material at http://link.aps.org/supplemental/10.1103/PhysRevLett.114.114505 for experimental setup and procedures.
[31] D. Axelrod, Traffic **2**, 764 (2001).
[32] T. Uchida, S. Oshita, M. Ohmori, T. Tsuno, K. Soejima, S. Shinozaki, Y. Take, and K. Mitsuda, Nanoscale Res. Lett. **6**, 295 (2011).
[33] P. G. de Gennes, F. Brochard-Wyart, and D. Quéré, *Capillarity and Wetting Phenomena: Drops, Bubbles, Pearls, Waves* (Springer, New York, 2004).
[34] P. G. de Gennes, Rev. Mod. Phys. **57**, 827 (1985).
[35] J. H. Weijs, J. H. Snoeijer, and D. Lohse, Phys. Rev. Lett. **108**, 104501 (2012).
[36] D. Bartolo, C. Josserand, and D. Bonn, Phys. Rev. Lett. **96**, 124501 (2006).
[37] T. D. Blake and J. De Coninck, Adv. Colloid Interface Sci. **96**, 21 (2002).
[38] T. D. Blake and J. M. Haynes, J. Colloid Interface Sci. **30**, 421 (1969).
[39] R. E. Johnson and R. H. Dettre, Adv. Chem. Ser. **43**, 112 (1964).
[40] C. Andrieu, D. A. Beysens, V. S. Nikolayev, and Y. Pomeau, J. Fluid Mech. **453**, 427 (2002).
[41] R. Narhe, D. Beysens, and V. S. Nikolayev, Langmuir **20**, 1213 (2004).
[42] R. Narhe, D. Beysens, and V. S. Nikolayev, Int. J. Thermophys. **26**, 1743 (2005).
[43] H. Schonhor, H. L. Frisch, and T. K. Kwei, J. Appl. Phys. **37**, 4967 (1966).
[44] S. Newman, J. Colloid Interface Sci. **26**, 209 (1968).
[45] J. H. Snoeijer and B. Andreotti, Annu. Rev. Fluid Mech. **45**, 269 (2013).